Solid Freeform Fabrication 2022: Proceedings of the 33rd Annual International Solid Freeform Fabrication Symposium – An Additive Manufacturing Conference
Reviewed Paper

Effect of laser polishing on fatigue behavior of additively manufactured IN718

Seungjong Lee[1,2], Martin Bureš[3], Shuai Shao[1,2], Douglas N. Wells[4], Miroslav Zetek[3], Miloslav Kepka[3], Nima Shamsaei[1,2*]

[1] National Center for Additive Manufacturing Excellence (NCAME), Auburn University, Auburn, AL 36849, USA

[2] Department of Mechanical Engineering, Auburn University, Auburn, AL 36849, USA

[3] Regional Technological Institute, University of West Bohemia, Univerzitní 8, 30614 Pilsen 30614, Czech Republic

[4] NASA Marshall Space Flight Center, Huntsville, AL 35812, USA

[*]Corresponding author: shamsaei@auburn.edu
Phone: (334) 844 4839

Abstract

This study investigates the effect of laser-polishing on the fatigue behavior of Inconel 718 fabricated using laser powder bed fusion process. Three different conditions including as-built and laser-polished using two different process parameters are considered. Uniaxial tension-compression fatigue tests are conducted in strain-controlled mode to examine the fatigue behavior for each condition. In addition, surface roughness measurements and fractography using optical microscopy and porosity measurements using the X-ray computed tomography are also performed for all conditions. The results indicate that laser-polishing alone does not improve fatigue performance, even though it can significantly reduce surface roughness. The beneficial effects of the smoother surfaces may have been countered by the volumetric defects close to the surface induced by laser-polishing. The fracture surfaces also reveal that fatigue cracks are initiated from the defects close to the surface, and therefore, fatigue behavior is not improved.

Keywords: Inconel 718; Laser powder bed fusion; Laser-polishing; Surface roughness; Fatigue

Introduction

Metallic additive manufacturing (AM), a layer-by-layer fabrication method, has received significant attention due to the feasibility of building complex geometries such as lattice structures that cannot be constructed by traditional subtractive manufacturing methods [1]. Laser powder bed fusion (L-PBF) is one of the well-known and popular AM methods because it provides arguably the most accurate built dimension and the least surface roughness (SR) through relatively thin layer thicknesses among various AM methods [2]. Although L-PBF fabricates geometrically precise parts, post-processing including thermal and surface treatments are still often applied required to employ L-PBF parts in engineering applications [3].

Inconel 718 (IN718) is a well-known nickel-base superalloy in many applications, such as in gas turbines due to its excellent mechanical properties and corrosion resistance [4]. However,

IN718 has high production costs owing to its expensive machinability [5]. Through the near-net-shaping capability of L-PBF, manufacturing of IN718 can achieve reduced machining costs and enable light-weighting. Therefore, IN718 fabricated by L-PBF technique has been studied by numerous researchers to verify practical applicability [6][7][8]. Gruber et al. [9] reported that L-PBF IN718 fabricated by optimized process parameters can have comparable hardness and tensile properties to wrought counterparts after appropriate heat treatments including stress relief, hot isostatic pressing (HIP), solution annealing, and standard double aging.

Although L-PBF fabricates parts with the smoothest surface among AM methods, the SR is still the most critical factor for fatigue properties. The fatigue lives of as-built (AB) L-PBF parts are significantly less than machined and polished counterparts because SR of AB L-PBF parts can act as micro-notches on the surface resulting in early fatigue crack initiations [11]. Therefore, post surface treatments are still required especially for fatigue critical applications. Lee et al. [12] studied the effects of various post surface treatments on fatigue behavior of L-PBF IN718 and reported that all post surface treatments including sand-blasting, drag-finishing, turning, and grinding can improve fatigue performance compared to the AB condition.

The post surface treatments, especially conventional techniques such as milling, turning, and grinding, can significantly improve fatigue performance. However, post surface treatments are not always feasible due to the complex geometries of the parts. In addition, these techniques hinder the benefits of AM which are fabricating complex geometries and near-net-shape parts within a single AM process. Laser techniques such as laser-polishing (LP) and laser-shock-peening have been employed as non-subtractive post surface treatment techniques for AM parts since they can reconstruct surface topography without wasting materials. Lee et al. [13] showed that the laser-polished L-PBF Ti-6Al-4V not only have better fatigue strength than AB counterparts but also have comparable fatigue lives to machined and polished counterparts.

The effects of LP on the fatigue behavior of L-PBF IN718 are examined in this study. Surface topographies and porosities of AB and LP specimens were measured followed by uniaxial strain-controlled fatigue testing to correlate the fatigue properties for each condition. The results show that LP successfully improves the surface quality of L-PBF IN718. However, LP processes generate defects close to the surface. As a result, LP specimens have similar fatigue lives compared to AB counterparts due to the defects close to the surface that introduce early crack initiations although the surface is smoother.

Experimental Procedure

IN718 fatigue specimens were fabricated using an EOS M290 L-PBF system in an argon atmosphere with the default process parameters provided by the manufacturer: laser power of 285W, laser scanning speed of 960 mm/s, hatching space of 110 μm, and layer thickness of 40 μm. According to ASTM E606, with the exception of the gage diameter of 5 mm [14], the geometry of specimens was designed as shown in Figure 1 and the specimens were fabricated vertically. One of the grips has a longer length to provide space to provide enough grip for the LP process. The specimens were heat treated based on ASTM F3301 and AMS 5564C: stress relief (1065°C for 1.5h followed by furnace cooling), solution treatment (1065°C for 1h, argon quenching), and two-step aging (760°C for 10h, furnace cooling to 650°C and holding for a total precipitation time of 20h) [15,16]. Two different LP conditions (i.e., LP1 and LP2) were processed by two different LP process parameters: LP1 – power of 400W, frequency of 600 Hz, scanning

speed of 100 mm/s, pulse duration of 0.5 ms, defocus of 14 mm and LP2 - power of 250 W, frequency of 700 Hz, scanning speed of 50 mm/s, pulse duration of 0.7 ms, defocus of 14 mm.

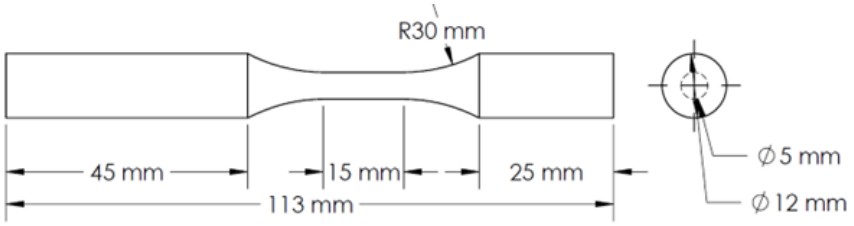

Figure. 1 Fatigue specimens' geometry according to ASTM E606.

Surfaces of AB, LP1, and LP2 specimens were scanned by a Keyence VHX-6000X optical microscope using 500X magnification with a scanned area of 2 mm by 1 mm. In order to obtain surface height data, a 3D stitching function was used. The captured 3D images were analyzed by software provided by Keyence. The 3D images were converted to the CSV files to calculate SR values using MATLAB.

The porosities of AB, LP1, and LP2 specimens were measured by Zeiss Xradia 620 Versa X-ray computed tomography (XCT) system. The gage sections with a diameter of 5 mm were scanned using the following settings: voltage of 160 kV, current of 156 μA, and voxel size of 5.5 μm. The scanned files are reconstructed by the software provided by Zeiss and saved as TIFF image files. The obtained TIFF image files were post processed by ImageJ and Dragonfly to visualize defects.

Fully reversed uniaxial strain-controlled fatigue tests with the constant strain rate of 0.0025 mm/mm/s were conducted on an MTS Landmark hydraulic system according to ASTM E606 [14]. Five different strain amplitudes (ε_a = 0.006, 0.005, 0.004, 0.003, and 0.0025 mm/mm) were tested for all three surface conditions to evaluate their influences in both low and high cycle fatigue regimes. If plastic deformation was not observed from the hysteresis loops during strain-controlled tests, the extensometer was removed after a few thousand cycles and the tests were switched to the force-control to reduce the testing times by increasing frequency.

Results and Discussion

The surface topographies of AB, LP1, and LP2 specimens generated by Keyence software are presented in Figure 2. The calculated SR values such as the arithmetical mean height (R_a), the maximum profile valley depth (R_v), and the maximum height of profile (R_z) are listed in Table 1. The AB specimen has partially melted powder particles and layer-wise undulations on the surface as shown in Figure 2(a). Both LP1 and LP2 not only removed partially melted powder particles but also reconstructed surfaces by remelting surfaces. As a result, R_a and R_v, which are considered important SR values in fatigue applications, are reduced by LP processes.

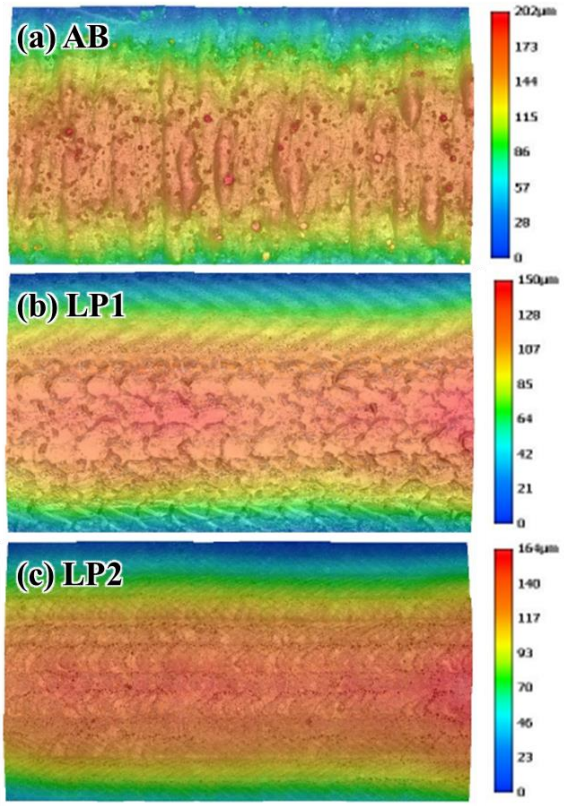

Figure. 2 Surface topographies of AB, LP1, and LP2 specimens overlaid with micrographs and colormaps.

Table. 1 The calculated SR values including R_a, R_v, and R_z of AB, LP1, and LP2 specimens.

Surface conditions	Surface roughness parameters		
	R_a (μm)	R_v (μm)	R_z (μm)
AB	4.75	12.23	39.19
LP1	2.91	8.12	18.32
LP2	2.35	9.16	19.54

Visualized XCT 3D images of AB, LP1, and LP2 specimens are presented in Figure 3 and porosity measurement results are listed in Table 2. AB specimens have significantly less defects in both number and size compared to LP1 and LP2 specimens. Interestingly, they have a similar number of defects in the center but LP1 and LP2 have slightly more defects close to the surface compared to AB, which were likely induced by the LP process itself. According to Table 2, the number of defects for both LPs was almost identical although the process parameters for LP1 and LP2 are different. The correlation might be that the total energy input per unit surface area for both parameters was kept almost the same to each specimen (LP1 ~0.2 J/mm^2 and LP ~0.175 J/mm^2) and therefore a similar melt pool depth and width due to LP processes might be expected. In order to remedy the LP process induced defects, HIP might be required as a post treatment, especially for fatigue critical applications.

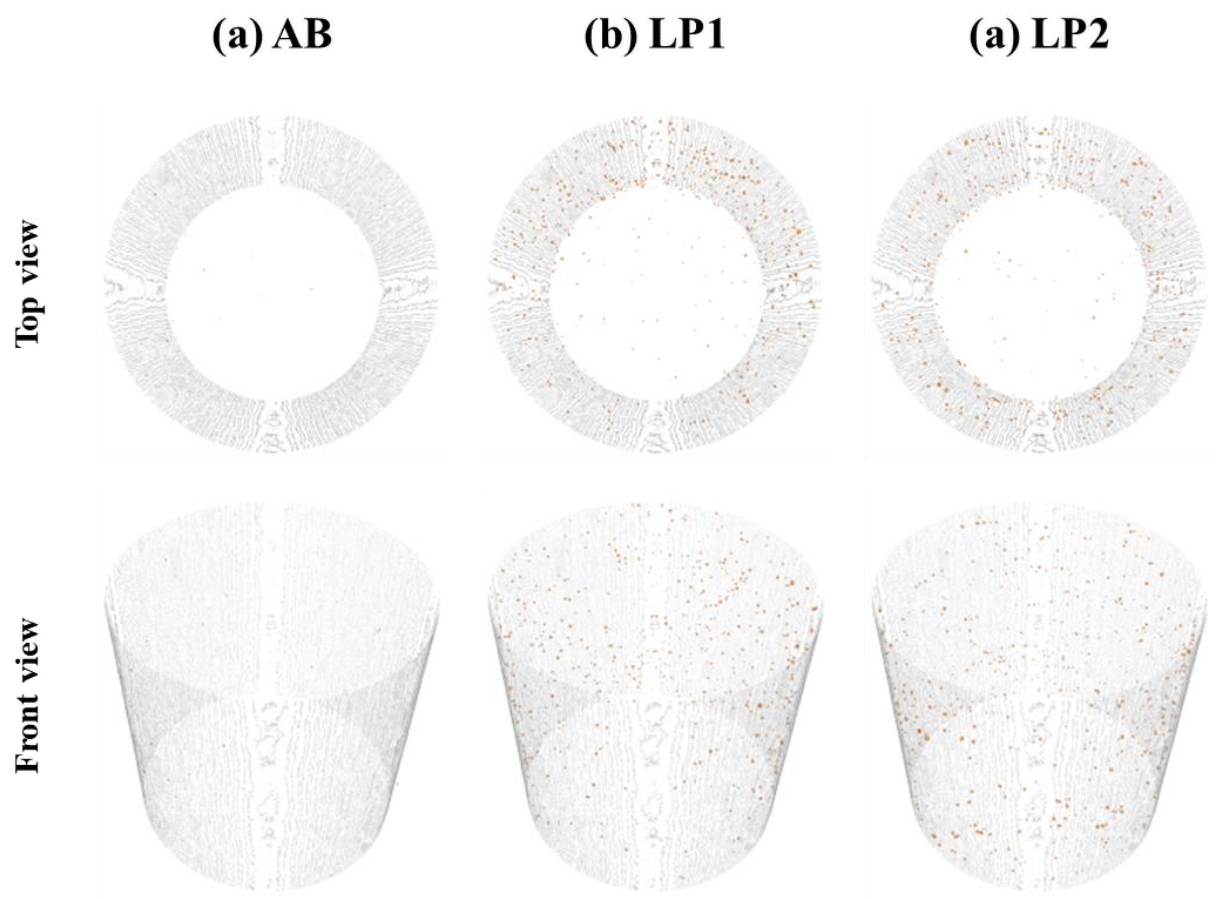

Figure. 3 Visualized XCT 3D images of AB, LP1, and LP2 specimens.

Table. 2 Porosity measurement results of AB, LP1, and LP2 specimens.

Surface conditions	AB	LP1	LP2
Number of defects	42	632	622
Maximum volume of defects (mm^3)	3.83E-05	1.21E-04	1.17E-04
Porosity (%)	0.0005	0.0074	0.0078

Strain amplitude versus reversals to failure fatigue plots of AB, LP1, and LP2 specimens are generated based on fully reversed uniaxial strain-controlled fatigue test results and presented in Figure 4. The effects of SR on fatigue behavior are typically significant in the high cycle regime since SR act as micro-notches that can induce early fatigue crack initiation [11]. However, LP1 and LP2 specimens have similar fatigue lives compared to AB specimens even in the high cycle regime (i.e., at ε_a = 0.003 and 0.002 mm/mm), although SR is decreased. Other surface treatments such as sand-blasting and drag-finishing were shown to successfully improve fatigue performance, although SR of them are similar to or even higher than LP1 and LP2 [12]. It indicates that other factors such as defects or tensile residual stresses induced by LP processes can hinder any expected improvements in fatigue strength due to the lower SR.

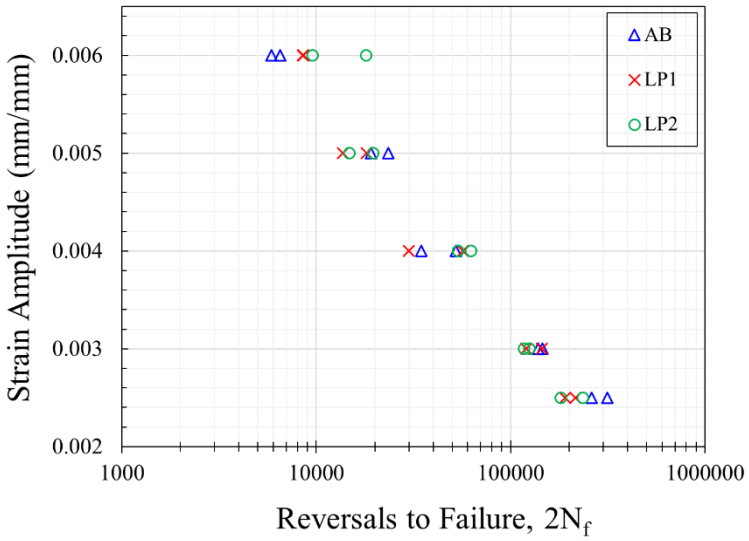

Figure. 4 Strain amplitude versus reversals to failure fatigue plots of AB, LP1, and LP2 specimens.

Fracture surfaces of AB, LP1, and LP2, specimens tested at the lowest strain amplitude (i.e., ε_a = 0.002 mm/mm) are presented in Figure 5. As shown in Figure 5(a), the AB specimen shows multiple crack initiation sites from the surface. LP1 and LP2 specimens not only have multiple crack initiation sites at the surface but also crack initiations from the defects close to the surface as shown in Figures 5(b) and (c). It confirmed that fatigue performances of LP1 and LP2 are not improved partly because of the defects close to the surface produced through LP processes. The two different process parameters utilized for LP processes were both prone to form defects. HIP process and two-step aging followed by LP processes can be suggested to close minimize defects without changing process parameters and improve fatigue strengths.

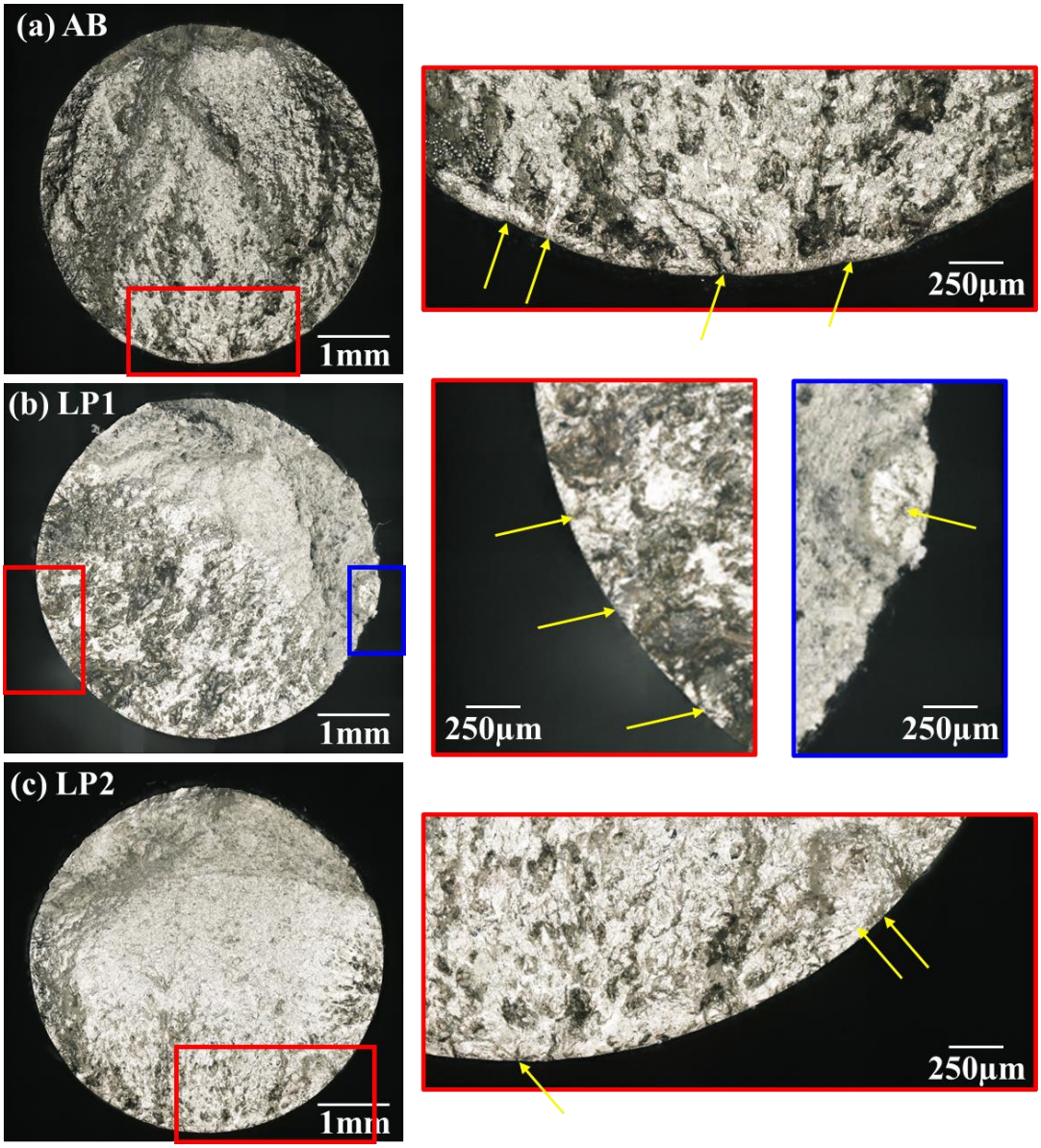

Figure. 5 Fracture surfaces of AB, LP1, and LP2, specimens tested at ε_a = 0.002 mm/mm (crack initiation sites are shown by the yellow arrows).

Conclusions

In this study, the effects of laser polishing on the fatigue behavior of L-PBF IN718 have been investigated. Two different laser polished surface conditions and the as-built surface condition were considered. Through surface and porosity measurements, fatigue tests, and fractography analyses, the following conclusions were drawn:

- The laser-polishing can remove partially melted powder particles and reconstruct surface topography by remelting the surface. The surface roughness of laser-polished specimens is lower than as-built specimens.
- The laser-polishing produced defects, which resulted in a higher number of defects near the surface in the melted layer. The laser-polishing process parameters such as defocus,

speed, power, and pulse duration should be considered in further study to reduce creating defects.

- Fatigue life cannot be improved by laser-polishing regardless of the process parameters of laser-polishing processes. Since the tensile residual stresses and defects produced by laser-polishing processes can cause early crack initiations resulting in shorter fatigue lives.
- Hot isostatic pressing is recommended to improve fatigue strengths by reducing defects close to the surface without changing laser-polishing process parameters.

Acknowledgment

This material is based upon work partially supported by the National Science Foundation (NSF) under grant # 1919818 and National Institute of Standards and Technology (NIST) under Award No. 70NANB18H220. The work also was supported from ERDF "Research of additive technologies for future applications in machinery industry - RTI plus" (No.CZ.02.1.01/0.0/0.0/18_069/0010040).

References

[1] Frazier WE. Metal additive manufacturing: A review. J Mater Eng Perform 2014;23:1917–28. https://doi.org/10.1007/s11665-014-0958-z.

[2] King WE, Anderson AT, Ferencz RM, Hodge NE, Kamath C, Khairallah SA, et al. Laser powder bed fusion additive manufacturing of metals; physics, computational, and materials challenges. Appl Phys Rev 2015;2:041304. https://doi.org/10.1063/1.4937809.

[3] Yadollahi A, Shamsaei N. Additive manufacturing of fatigue resistant materials: Challenges and opportunities. Int J Fatigue 2017;98:14–31. https://doi.org/10.1016/j.ijfatigue.2017.01.001.

[4] Amato KN, Gaytan SM, Murr LE, Martinez E, Shindo PW, Hernandez J, et al. Microstructures and mechanical behavior of Inconel 718 fabricated by selective laser melting. Acta Mater 2012;60:2229–39. https://doi.org/10.1016/j.actamat.2011.12.032.

[5] Rahman M, Seah WKH, Teo TT. The machinability of Inconel 718. J Mater Process Technol 1997;63:199–204. https://doi.org/10.1016/S0924-0136(96)02624-6.

[6] Jia Q, Gu D. Selective laser melting additive manufacturing of Inconel 718 superalloy parts: Densification, microstructure and properties. J Alloys Compd 2014;585:713–21. https://doi.org/10.1016/j.jallcom.2013.09.171.

[7] Wang X, Gong X, Chou K. Review on powder-bed laser additive manufacturing of Inconel 718 parts. Proc Inst Mech Eng Part B J Eng Manuf 2017;231:1890–903. https://doi.org/10.1177/0954405415619883.

[8] Hosseini E, Popovich VA. A review of mechanical properties of additively manufactured Inconel 718. Addit Manuf 2019;30:100877. https://doi.org/10.1016/j.addma.2019.100877.

[9] Gruber K, Stopyra W, Kobiela K, Madejski B, Malicki M, Kurzynowski T. Mechanical properties of Inconel 718 additively manufactured by laser powder bed fusion after industrial high-temperature heat treatment. J Manuf Process 2022;73:642–59.

https://doi.org/10.1016/j.jmapro.2021.11.053.

[10] Fatemi A, Molaei R, Simsiriwong J, Sanaei N, Pegues J, Torries B, et al. Fatigue behaviour of additive manufactured materials: An overview of some recent experimental studies on Ti-6Al-4V considering various processing and loading direction effects. Fatigue Fract Eng Mater Struct 2019;42:991–1009. https://doi.org/10.1111/ffe.13000.

[11] Lee S, Pegues J, Shamsaei N. Fatigue Behavior and Modeling for Additive Manufactured 304L Stainless Steel: The effect of Surface Roughness. Int J Fatigue 2020;141:105856. https://doi.org/10.1016/j.ijfatigue.2020.105856.

[12] Lee S, Shao S, Wells DN, Zetek M, Kepka M, Shamsaei N. Fatigue behavior and modeling of additively manufactured IN718: The effect of surface treatments and surface measurement techniques. J Mater Process Technol 2021;302:117475. https://doi.org/10.1016/j.jmatprotec.2021.117475.

[13] Lee S, Ahmadi Z, Pegues J, Mahjouri-Samani M, Shamsaei N. Laser Surface Treatment for Improving Fatigue Performance of Additive Manufactured Ti-6Al-4V Parts. Opt Laser Technol 2020:Under Review.

[14] ASTM E606. ASTM E606 Standard Test Method for Strain-Controlled Fatigue Testing. ASTM Stand 2021. https://doi.org/10.1520/E0606_E0606M-21.

[15] ASTM F3301. Standard for Additive Manufacturing – Post Processing Methods – Standard Specification for Thermal Post-Processing Metal Parts Made Via Powder Bed Fusion. ASTM Stand 2018:3. https://doi.org/10.1520/F3301-18A.2.

[16] AMS 5564. STEEL TUBING, CORROSION RESISTANT 19Cr - 10Ni (SAE 30304) High Pressure Hydraulic, Welded Plus Ultrasonically Tested or Seamless 2013.